DRYING TECHNOLOGY

ISSN: 0737-3937 (Print) 1532-2300 (Online) Journal homepage: http://www.tandfonline.com/loi/ldrt20

FROM SINGLE PARTICLE TO FLUID BED DRYING KINETICS

Evangelos Tsotsas

To cite this article: Evangelos Tsotsas (1994) FROM SINGLE PARTICLE TO FLUID BED DRYING KINETICS, DRYING TECHNOLOGY, 12:6, 1401-1426, DOI: 10.1080/07373939408961013

To link to this article: https://doi.org/10.1080/07373939408961013

Published online: 21 May 2007.

DRYING TECHNOLOGY, 12(6), 1401-1426 (1994)

FROM SINGLE PARTICLE TO FLUID BED DRYING KINETICS

Evangelos Tsotsas
Dow Deutschland Inc
Solids Processing Engineering Science Lab
Postfach 1120, 21677 Stade, Germany

Dedicated to Prof. Dr.-Ing. Dr.h.c./INPL Ernst-Ulrich Schlünder on the occasion of his 65th birthday

Key Words and Phrases: drying curves; fluidization; heterogeneous model, normalization, single particles; particulates

ABSTRACT

The concept of a normalized single particle drying curve has been integrated into a generic, heterogeneous fluid bed model in order to describe batch fluid bed drying. Drying curves have been measured for both single particles and fluid beds. Two different coarse-grained materials, aluminum silicate and a technical product, have been used. In general, fluid bed drying curves appear to be predictible on the basis of single particle data and with the help of the model. Dificulties may arise mainly with particles of low sphericity and a large initial moisture content. Model parameters are in the range indicated by general fluidization literature. However, Sherwood numbers for particle-to-fluid mass transfer in the fluid bed are significantly lower than the values for single particles. This can hardly be attributed to bubbling and bypassing, since these effects have been explicitly accounted for in the model.

INTRODUCTION AND SCOPE

In spite of its great practical importance in the chemical industry and the large volume of literature available on general fluidization issues, the number of papers published on fluid bed drying is rather limited. While some authors adopt an empirical approach [1] other workers try to describe fluid bed hydrodynamics more precisely by transferring methods developed for the design of fluid bed reactors to the drying problem [2,3,4]. Combinations of flow modelling with empirical findings have also been proposed [5].

One restriction of existing results is that they refer mostly to small particles. On the other hand, the pool of published data which could be used for a reasonable comparison with models is rather meagre. Finally, and this appears to be the most serious shortcoming, the distinction between gas-side and particle-side kinetics is usually poor. In the present work we attempt to sharpen this distinction by using the concept of normalization as proposed by van Meel [6] and applied by various authors, especially by Schlünder and co-workers [7,8]. Doing so, three constituent items of the fluid bed drying problem may be identified:

- **A** : The fluid bed drying curve, a variable depending on product properties as well as on operating conditions.
- **B** : The normalized single particle drying curve. According to [6-8] this is - at least approximately - a constant, characterizing uniquely particle-side drying kinetics.
- **C** : A model describing flow, particle motion and gas-side transport phenomena in the fluid bed.

On the basis of these three constituents three different types of investigations may be conducted:

1. Determination of fluid bed drying curves (A) from the normalized single particle drying curve (B) of the product under consideration and the fluid bed model model (C).
2. Derivation of the normalized single particle drying curve (B) with the help of the fluid bed model (C) from a set of fluid bed drying curves (A).
3. Derivation of the fluid bed model (C) from fluid bed (A) as well as single particle (B) data.

The above three cases are depicted schematically in Fig. 1. Full circles and arrows denote known items, empty unknown ones. Evidently, if only one item is known, the derivation of the other two is

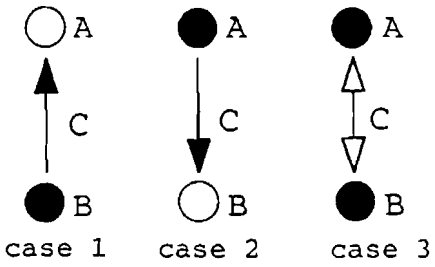

FIGURE 1. Fluid bed drying kinetics (A), single particle kinetics (B) and fluid bed model (C) are interconnected items. Two of them must be known (full circles/arrows) in order to reliably predict the third

risky. Therefore, and to our knowledge for the first time in literature, we tried to remove one degree of freedom from the problem by determining two of its three constituents experimentally. In specific terms, the present work tries to realize the above case 3 by measuring directly both single particle as well as fluid bed drying curves. Our goal is to find out:

- Whether it is possible to connect single particle with fluid bed phenomena with a mathematical fluid bed model
- How complicated this model has to be
- which values the model parameters have, and if they agree with other relevant values from the literature

The successful completion of the investigation would open our way to case 1, which is the scale-up to industrial dimensions. It would also open the way to case 2, i.e. to the derivation of the normalized single particle drying curve from lab fluid bed data. This is an important step with fine grained materials which can not be investigated experimentally on the single particle level. The combination of case 1 with case 2 is nothing but the "double-scaling procedure" as discussed in [9]. It comprises all aspects of the design of convective dryers, not only of the fluid bed type.

MATERIALS

A model substance and a technical product differing primarily in the particle shape have been used in the present investigation.

The model substance is aluminum silicate in form of hard, capillary porous and almost perfectly spherical particles. While single particle measurements have been conducted with several particle sizes, a narrowly sieved fraction with an average particle diameter of $d = 1.44$ mm has been used in all fluid bed runs. The dry particle density is 1667 kg/m^3, the packed bed density about 1000 kg/m^3 with a typical packed bed porosity of 0.40. Pressure drop measurements and calculations located the onset of fluidization for the dry substance at a superficial gas velocity of about $u_L = 0.55$ m/s.

The technical product consists of porous, extremely non-spherical, flake-like particles. It is lighter than aluminum silicate and, in terms of equivalent particle diameter, coarser. Fluidization of the dry bed occurs at about $u_L = 1.1$ m/s.

With both materials the same sample has been used throughout the investigation, by rewetting after every run. The moisture has been distilled water, the drying agent air. The technical product as well as aluminum silicate are only slightly hygroscopic in respect of water. This small hygroscopicity has been neglected for the purpose of the present work. No negative impact of particle moisture on the quality of fluidization has been observed.

EXPERIMENTAL

Three different experimental facilities have been used.

- Analytical balance for single particle runs

Wet single particles were put on a high-accuracy analytical balance and left to dry out under room conditions (about 25 °C, about 60% relative humidity). A personal computer connected to the balance calculated immediately the single particle drying curve, i.e. the functional dependence between the drying rate m_{sp} and the dry-based particle moisture content X.

- Drying channel

Single particles hanging on the downfloor side of a balance were dried in a channel. Weight changes and time were recorded during the run and then transformed to the single particle drying curve $m_{sp}(X)$. The measuring section of the drying channel was rectangular (150x150 mm). Inlet air was dehumidified with zeolite and was essentially free of moisture.

Accuracy and handling limit the applicability of both the channel and the analytical balance to particles larger than about 1 mm.

• Batch fluid bed dryer.

A flowsheet of the batch fluid bed dryer is depicted in Fig. 2. Air is supplied by a blower and treated by a dehumidifier (DB) to a dew point lower than -30 °C before entering the conditioning section (AC). There the desired flow rate and temperature are adjusted. The fluidization vessel (FB) is made of glass and has an inner diameter of 150 mm. A perforated plate distributor is used, providing sufficient pressure drop for a good operation. A second perforated plate - not depicted in Fig. 2 - serves as predistributor. The valves V1 and V2 allow to supply the fluid bed with air or, alternatively, bypass it. A short bypass period is necessary in order to fill-in the material, just before starting a drying experiment.

Several temperatures and pressures are measured. However, the core instrument of the rig is a Rosemount IR-analyzer (GA) determining the water vapour content in the outlet air continuously and without significant time delay. To this purpose a small air stream is bypassed at the top of the apparatus and pumped to the gas analyzer. Conduits, the pump and the analyzer itself are tempered in order to prevent condensation and increase accuracy. All data are collected by a data acquisition system Camile 2000 (Trademark of the Dow Chemical Company). The outlet air vapour content versus time curve is transformed by the host personal computer to the fluid bed drying curve $m_{fb}(X)$. A sampling tube for the determination of local bed temperatures and air moisture contents (TI1, MI2) is available, but has not been used in the present work.

The calibration of the flowmeter (FI1) and of the gas analyzer has been checked with very good results. An overall control has been conducted for every drying experiment by means of the total water balance. The amount of water is determined by weighing the solids before and after the run, as well as from the integral of the water vapour content in the outlet air measured by the IR. The deviation between the two measurements was always within ±5%, mostly lower.

SINGLE PARTICLE DRYING CURVES

Selected single particle drying curves are shown in Figs 3, 4. The aluminum silicate measurements of Fig. 3 were conducted on the

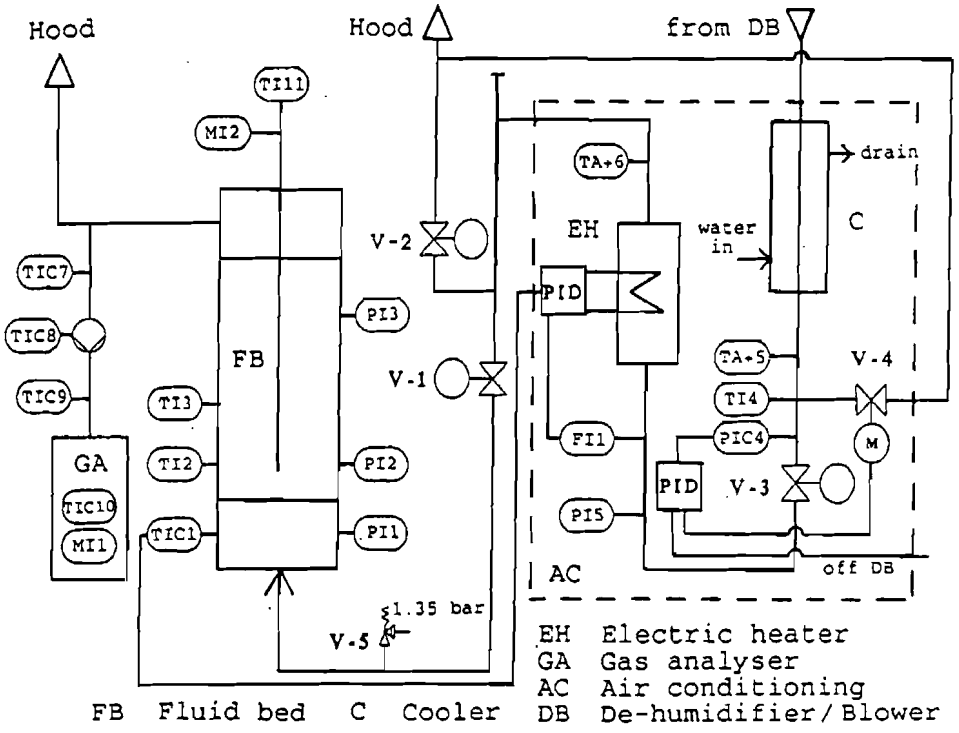

FIGURE 2 Flowsheet of batch fluid bed dryer

analytical balance, while the results of Fig 4 with the technical product were gained in the drying channel. Channel data scatter, because some movement of the particle and its supporting thread in the air flow can not be avoided and impacts the balance. In spite of this, reproducibility is good on average (compare the two runs conducted at 60 °C in Fig 4).

For both products the first drying period is clearly decernible. Hence, the respective constant drying rate $m_{sp,I}$ as well as the critical moisture content X_{cr} can be dermined. We obtain $X_{cr} = 0.11$ for aluminum silicate and $X_{cr} = 0.55$ for the technical product. On this basis the normalization suggested in [6-8] can be carried out. The

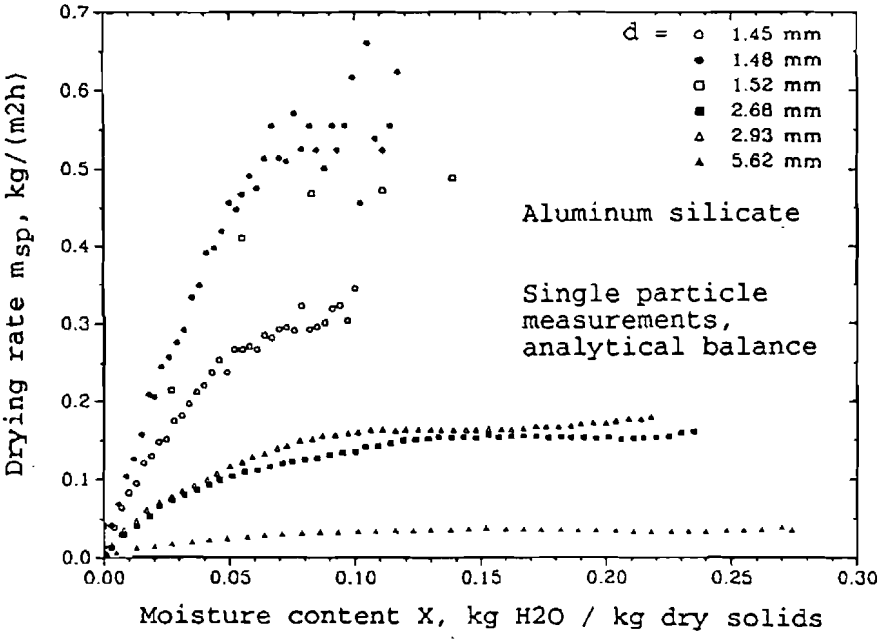

FIGURE 3. Single particle drying curves for aluminum silicate on analytical balance

normalized drying rate ν and solids moisture content η are defined as

$$\nu = m_{sp} / m_{sp,I} \quad , \tag{1}$$

$$\eta = (X - X_{eq}) / (X_{cr} - X_{eq}) \tag{2}$$

X_{eq} is the equilibrium moisture content of solids at the prevailing drying conditions. In our case of negligible hygroscopicity $X_{eq} = 0$.

Remember that drying is assumed to be gas-side controlled in the first and particle-side controlled in the second drying period (at $X < X_{cr}$). By normalization the two periods are separated from each other. Gas-side phenomena (i.e. the drying rate $m_{sp,I}$) are supposed to be predictible from first principles. Particle-side phenomena are

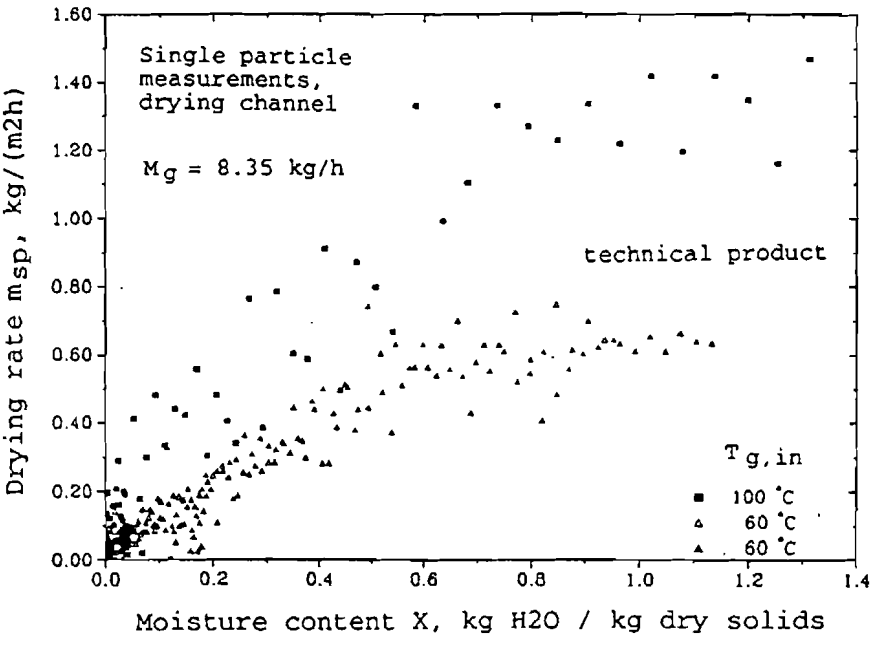

FIGURE 4. Single particle drying curves for technical product in drying channel.

described empirically by the function $\nu(\eta)$. Successful normalization leads to a function $\nu(\eta)$ which is invariant upon drying conditions and, thus, characterizes the drying behaviour of the product under consideration uniquely

Since the concept of normalization is empirical, its applicability must be tested from case to case. For our products normalization appears to work quite well. As we see in Fig. 5 all aluminum silicate data from Fig 3 can be described within technical accuracy by one and the same curve As an approximation, four straight segments covering the interval $0 < \eta < 1$ are used in Fig. 5. For $\eta > 1$ it is per definition $\nu = 1$ (eqs(1),(2)). Drying channel measurements with aluminum silicate have not been done in the present work. However, a couple of such measurements have been reported by Schwarzbach [10]. Normalization of these results - not depicted here - revealed a very encouraging agreement with the fitting curve of Fig. 5.

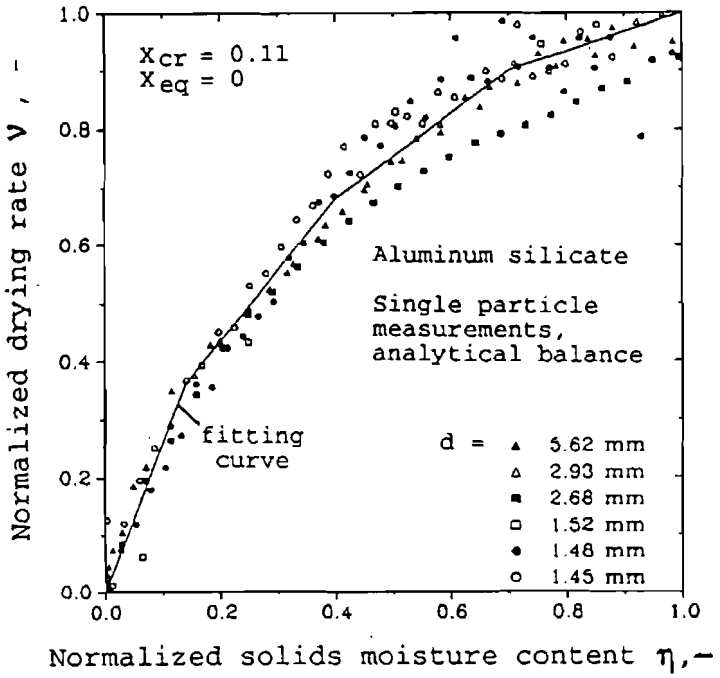

FIGURE 5. Normalized single particle drying curve of aluminum silicate

The single particle drying curves of the technical product from Fig. 4 are plotted in Fig. 6 in their normalized form. Again, all curves collapse with acceptable accuracy. On the one hand, the primary data of Fig. 4 are already subjected to considerable experimental scatter, on the other every single particle of a technical product is somewhat different than the other particles. In Fig. 6 the function $\nu(\eta)$ is fitted by $\nu(\eta) = \eta$, i.e. by the diagonal of the plot. This is a simple rule-of-thumb choice. It appears to slightly underestimate drying rates at small moisture contents, being moderately conservative in respect of practical use.

Difficulties with normalization will arise with materials without a measurable first drying period. In such cases the calculation of $m_{sp,I}$ from first principles is be recommended. This is quite easy

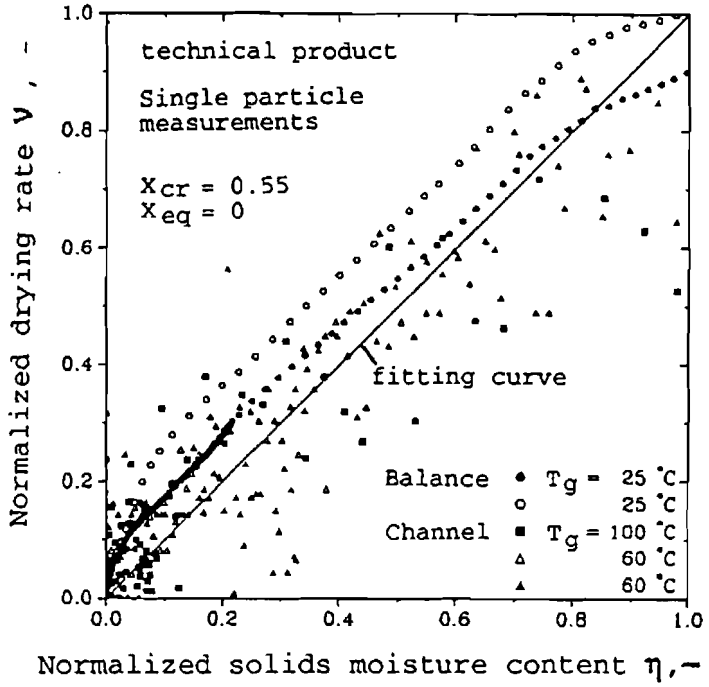

FIGURE 6. Normalized single particle drying curve of technical product

and reliable for drying channel conditions. In a second step, the measured drying curves can be extrapolated and X_{cr} derived. The prediction of $m_{sp,l}$ for analytical balance conditions is uncertain Presumedly, heat transfer from the plate of the scale to the particle through the respective gas gap is of importance. This topic is not followed further in the present investigation.

FLUID BED DRYING CURVES

Fluid bed drying results are presented in Figs 7, 8 and 9. In Fig. 7 fluid bed drying curves for aluminum silicate at three different static bed heights h_0 are plotted. Inlet air temperature has been $T_{g,in}$ = 40

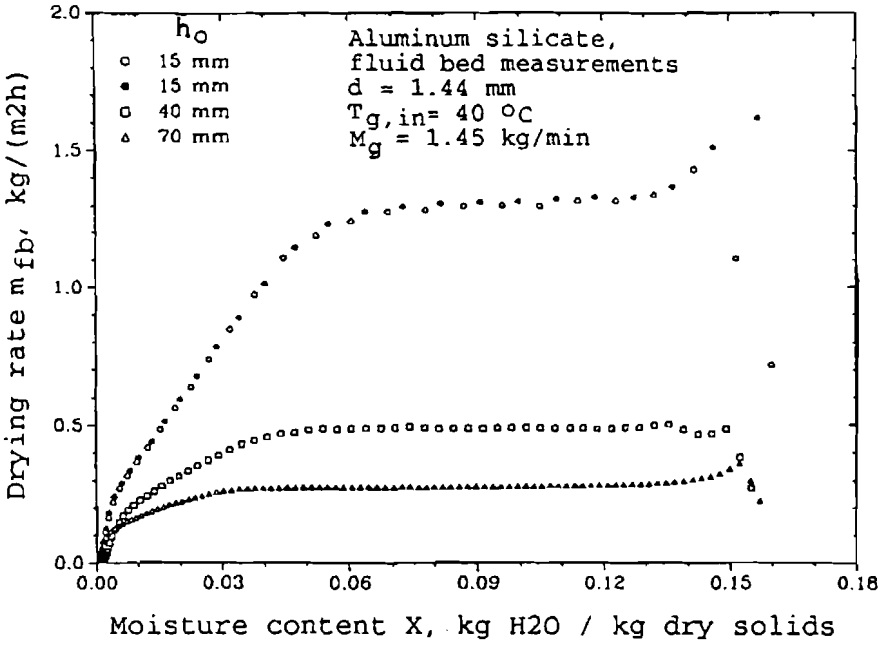

FIGURE 7. Fluid bed drying curves for aluminum silicate. Low air flow rate

°C, air mass flow rate M_g = 1.45 kg/min in these measurements. The drying rate m_{fb} refers to the total particle surface of the bed. Decreasing bed height leads to a lower average vapour concentration in the gas phase and, therefore, to an increased drying rate. For only one particle layer maximal drying rates would have been obtained. As Fig 7 shows the fluid bed drying curves also possess a constant and a falling rate period. However, these are not identical to the first and the second drying periods of single particle drying. Actually, the "critical" moisture content in a fluid bed decreases with increasing static bed height (hold-up), an effect which has been thoroughly discussed in [9]. As the two different runs at h_0 = 15 mm reveal, reproducibility is excellent.

The measurements of Fig. 7 have been repeated at a considerably larger air mass flow rate (M_g = 3.11 kg/min). Respective results are

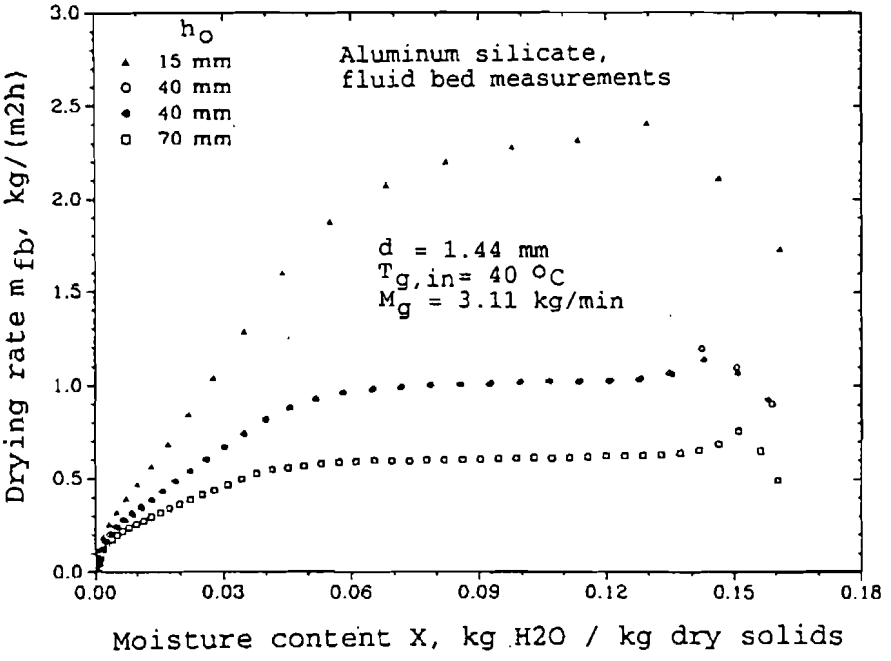

FIGURE 8. Fluid bed drying curves for aluminum silicate High air flow rate

plotted in Fig 8 As expected, the drying process is enhanced by increasing the air flow rate. Reproducibility is, again, very satisfying (see the two runs at h_0 = 40 mm)

Results for the technical product at $T_{g,in}$ = 40 °C, M_g = 2.75 kg/min and three different values of h_0 are depicted in Fig. 9 Here, the drying rate experiences a rather sharp decrease at medium solids moisture contents. At the end, relatively low drying rates are observed which decrease almost linearly with X. The impact of static height h_0 is similar as for aluminum silicate. Satisfactory, though not perfect reproducibility is observed. Further runs with the technical product - not depicted here - have been conducted at $T_{g,in}$ = 80 °C. As expected, the drying rate increases with increasing inlet air temperature

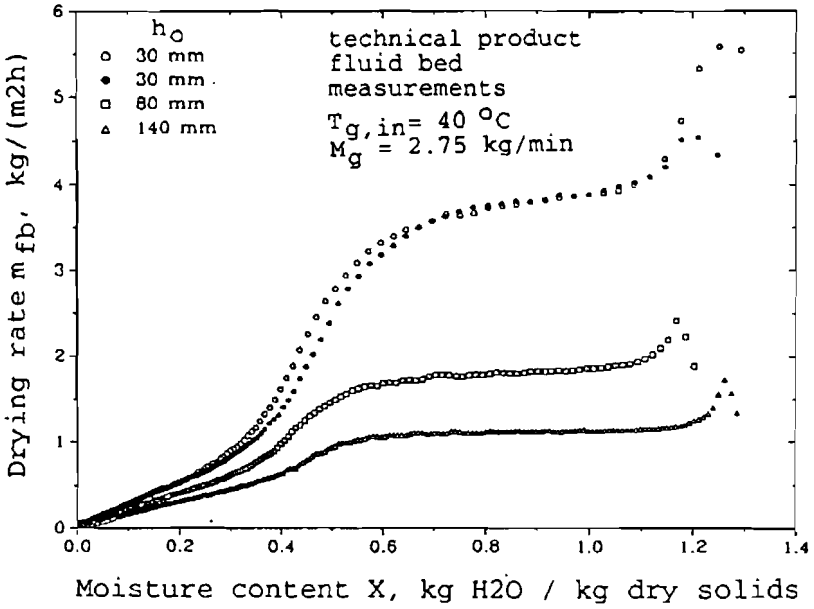

FIGURE 9. Fluid bed drying curves for technical product

The sum of our fluid bed measurements, together with comparable results from the literature, confirm the large variability of fluid bed drying curves upon drying conditions and hold-up. The common practice of measuring a couple of fluid bed drying curves in the lab and designing industrial convective dryers based on them can be severely misleading. As pointed out in the introduction, only single particle data can be scaled-up in a reliable way.

THE MODEL

In order to describe the batch fluid bed drying process the normalized single particle drying curve is incorporated into a heterogeneous fluid bed model distinguishing between a suspension and a bubble phase. A similar approach has been proposed by May [11] for fluid bed reactors and has, since, been further elaborated by

various authors (see the review by Werther [12]). The model assumptions, which are schematically recapitulated in Fig. 10 are as follows:

- The bubble phase is free of particles. The gas is flowing in ideal plug flow
- Vapour transport takes place between the suspension and the bubble phase
- All solids are in the suspension phase. They are perfectly backmixed.
- The gas of the suspension phase may be either perfectly backmixed or in ideal plug flow. Present results are based on the ideal plug flow version
- Mass transfer between the surfaces of the particles and the gas is taking place in the suspension

Mass balances are written down locally for each phase and integrated over the bed height, accounting for the coupling between the phases. Closed solutions are obtained. In this way the outlet air moisture content and the fluid bed drying rate can be calculated for any given value of X. Repeating the calculation at various solids moisture contents complete fluid bed drying curves are obtained.

Here, we will refrain from giving derivations or formulae (see [13]). However, it should be pointed out that all flow and gas-side mass transfer phenomena are described by the following three parameters:

- The bypass ratio v which is the ratio of air flowing through the bubbles to the total air flow rate

- The number of transfer units for mass transfer between suspension and bubbles NTU_i, defined as

$$NTU_i = \rho_g \beta_i A_b / M_g \tag{3}$$

with the mass flow rate of dry gas (air) M_g, the gas density ρ_g, the total surface area of the bubbles A_b, and the respective mass transfer coefficient β_i

- The number of transfer units for mass transfer from the particle surface to the gas NTU_g, according to the definition

$$NTU_g = \rho_g \beta_g A / M_g \tag{4}$$

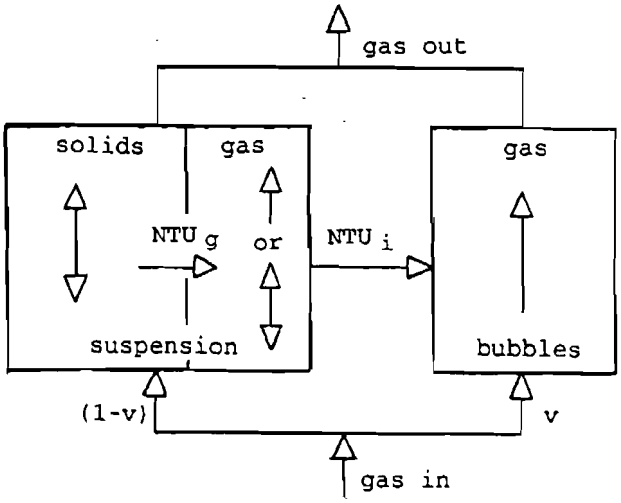

FIGURE 10. Scheme of the fluid bed model

Here A and β_g are the total particle surface area and the relevant mass transfer coefficient, respectively

As already explained, all intraparticle transfer phenomena are represented by the normalized single particle drying curve $\nu(\eta)$

The model is versatile, including several often used variants as limiting cases So, by putting $v = 0$ bubbling is neglected. A homogeneous bed is obtained also at NTU_i going to infinity In contrary, by setting $NTU_i = 0$ the bubbles are assumed to cross the bed without picking up any moisture (inactive bypass)

THE MODEL PARAMETERS AND THE PREDICTION OF FLUID BED DRYING CURVES

In the preceeding sections considerable progress has been made in collecting the material necessary for the calculation according to case 3, as discussed in the introduction: Item A (a set of fluid bed drying curves) as well as item B (the normalized single particle drying curve) are at our disposal, both from direct measurements, and for

both products considered. A generic fluid bed model (item C) has also been developed. Now, it remains to find out whether the pieces of the fluid bed drying problem fit together, and, if they do, what the exact form of the fluid bed model and the values of its parameters must be.

For the model substance aluminum silicate a number of preliminary calculations have been conducted. These will not be presented here; a separate communication is planned to this purpose. The result is that the fluid bed drying curves can not be satisfactorily predicted on the basis of the single particle kinetic data by any simplified variant of the model (i.e. no bypass, inactive bypass etc). Evidently, the bubbling behaviour and the mass transfer between the suspension phase and the bubbles have to be accounted for. I.e., it is necessary to use the full heterogeneous model. With the latter, predicted fluid bed drying curves can be obtained which are - from the practical point of view - accurate enough.

Some predicted drying curves of this kind are plotted and confronted with the measurements in Figs. 11 and 12. Fig. 11 corresponds to Fig. 7 (small air flow rate) and Fig. 12 to Fig. 8 (large air flow rate). The difference in the presentation is caused by the orginate of the graphs. Now, the reduced quantity

$$m_{fb}^{-} = m_{fb} / m_{fb,s} \qquad (5)$$

is used in the place of the dimensional fluid bed drying rate m_{fb}. The denominator of eq.(5) ($m_{fb,s}$) is defined as that drying rate which would correspond to complete saturation of the outlet air. It has been calculated from the adiabatic saturation temperature for the prevailing drying conditions. Consequently, m_{fb}^{*} is a kind of efficiency-ranging between zero and unity.

The new presentation reveals that a couple of points in the beginning of each run lie above saturation. However, the effect is so small, that no special effort was undertaken to explain it. Another result of the reduction by $m_{fb,s}$ is that the total particle surface area is eliminated from the ordinate. Consequently, the impact of static bed height h_0 is inversed in respect to Figs. 7, 8. Now, the drying curves with a large static bed height lie - as intuitively expected - on the top. On the other hand, the distance to saturation is enlarged by

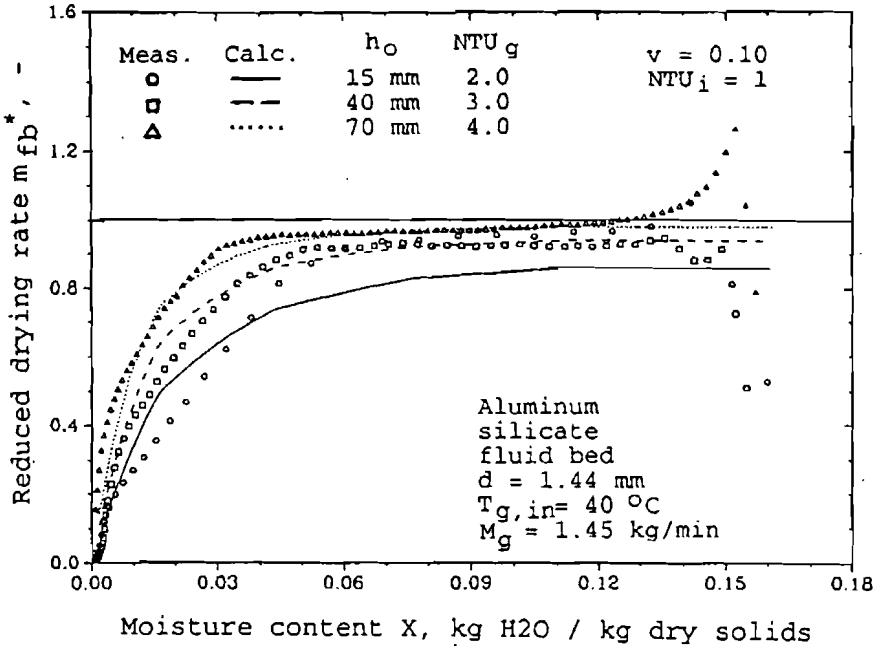

FIGURE 11. Measured and calculated fluid bed drying curves Aluminum silicate, low air flow rate.

increasing the air mass flow rate M_g (compare Fig. 11 with Fig. 12)

Concerning the model parameters the following is of importance:

- According to the fluidization literature (e.g. [14,15]) the bypass ratio v for small and light particles belonging to group A of Geldart's classification should be approximately equal to the excess ratio v_E defined as

$$v_E = (u_0 - u_L) / u_0 \qquad (6)$$

Consequently all air additional to that necessary for incipient fluidization should flow through the bubbles. The large and rather heavy aluminum silicate particles correspond, however, to Geldart's group D. For such materials v is expected to be only a small fraction of v_E,

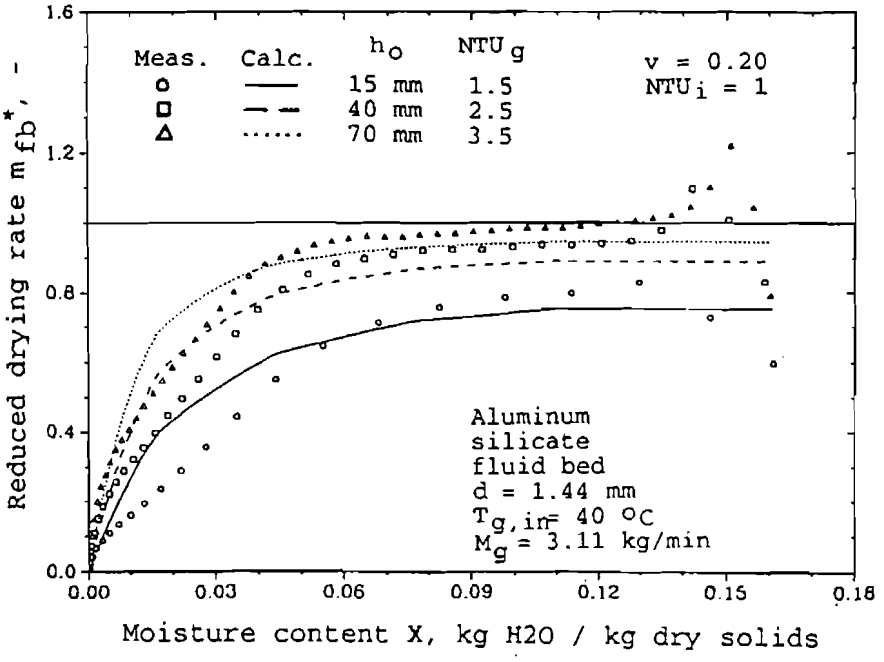

FIGURE 12. Measured and calculated fluid bed drying curves Aluminum silicate, high air flow rate

whereby values of

$$v = (0.20 \text{ to } 0.25)\, v_E \qquad (7)$$

appear reasonable [14,15]. In Figs 11 and 12 v = 0.10 and v = 0.20 have been used for the low and the high air flow rate, corresponding to superficial velocities at inlet temperature of u_0 = 1.23 m/s and 2.63 m/s, respectively. Taking into account that the incipient fluidization velocity for the wet product is somewhat larger than for the dry one - i.e. somewhat larger than the previously mentioned u_L = 0.55 m/s - we see that our bypass ratios cope well with eqs (6),(7). Note that the program implementing the fluid bed model can follow up the change of u_L and v with decreasing solids moisture content X. However, no use of this option has been made in the present work. Instead, the values of v

= 0.10 resp 0.20 have been kept constant throughout the drying process

- A number of mass transfer units between suspension and bubbles of $NTU_i = 1$ has been used throughout the calculations. This is located well in the middle of what is known from the literature on this subject for our actual conditions [12,14].

- The parameters v and NTU_i have been rather set on the basis of existing literature than fitted. Real fitting took place only in respect of the number of units for particle-to-fluid mass transfer NTU_g. Values of NTU_g = 1.5 to 4.0 have been obtained, see Figs 11, 12, depending on the static bed height h_0. These can be assessed best when converted to Sherwood numbers $Sh_g = \beta_g d/\delta$ and plotted against the Reynolds number $Re_0 = u_0 d/\nu_g$; (δ: diffusion coefficient and ν_g: kinematic viscosity in the gas). Results are shown in Fig. 13, as open cicles. Note that three different Sh_g-values are obtained at each Reynolds number, because a residual influence of bed height h_0 is still present. Such an impact is theoretically not permitted and could, actually, have been eliminated in the fitting procedure without significantly disturbing the overall agreement with the measured fluid bed drying curves. In Fig. 13 predictions according to the VDI-Wärmeatlas [16] for a single sphere (porosity $\psi = 1$) as well as for a packed bed of spherical particles ($\psi = 0.40$) are also depicted (solid lines). In the same time the findings of several authors for fluid beds, as collected by Schwarzbach [10], are represented by the shaded area. The following should be pointed out:

- Our Sh_g-values for aluminum silicate are in good company of many other results from the literature. However, the agreement should not be overestimated since differences exist in the experimental methods and in the models used for evaluation.
- The Sherwood numbers are significantly lower than the predictions of VDI-Wärmeatlas [16]. Using the latter a satisfactory derivation of fluid bed drying kinetics from single particle data could not be attained.
- The small Sherwood numbers can not be explained by bypassing as suggested in [10,17]. Though bubbling is explicitely accounted for in the model, small Sherwood numbers are still necessary.

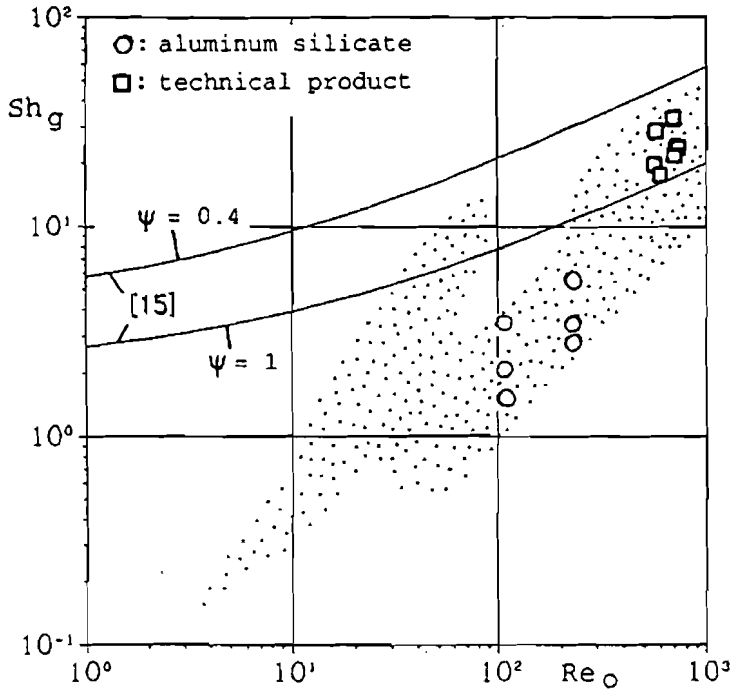

FIGURE 13. Particle-to-gas Sherwood numbers Sh_g.

- Axial dispersion in the suspension gas can neither explain the deviation from the single particle curve completely. Respective calculations have been conducted by using the ideal backmixing version of the model and will be presented elsewhere. The results of these calculations could not be brought into satisfactory agreement with the measured fluid bed drying curves. In this context differences in the behaviour appear to exist between fluid and fixed beds (compare with [18]).
- A thorough satisfying theoretical explanation of gas-side mass transfer in fluid beds can not be given at this time.

For the technical product accurate fluid bed drying curves can also been obtained, as illustrated in Fig. 14 (corresponding to Fig. 9). To this purpose, again, the full, heterogeneous fluid bed model must be used. NTU_i has been kept at the reasonable value of $NTU_i = 1$. And, the bypass ratio is $v = 0.10$, coping well with eqs (6),(7). In this context,

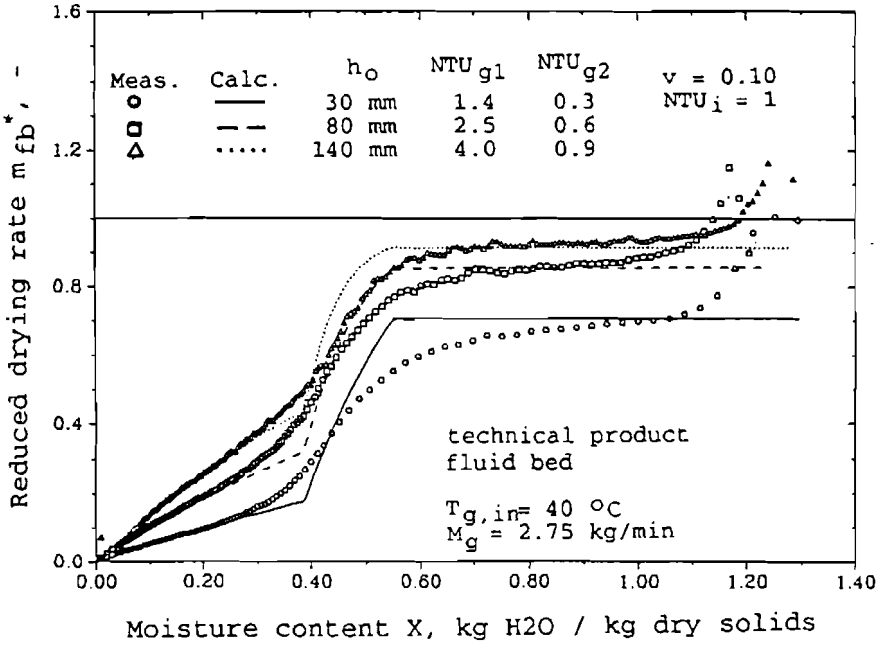

FIGURE 14. Measured and calculated fluid bed drying curves for technical product

note that fluidization of the wet product will set on at a larger velocity than the 1.1 m/s mentioned previously for the dry one.

In the beginning of drying the particle-to-gas mass transfer units have been fitted to NTU_{g1} = 1.4, 2.5 and 4.0, depending on static bed height h_0. The same values have been used also for measurements at the larger inlet air temperature of $T_{g,in}$ = 80 °C (not shown here). In this way, six Sherwood numbers result which are plotted in Fig. 13 with open squares. Again, a small influence of bed height is still present in Sh_g. This could have been eliminated without impacting the quality of fit significantly. One important difference to aluminum silicate is that, now, the Sherwood numbers lie there, where fluid bed data are expected to be. Namely, between the VDI-Wärmeatlas predictions for a packed bed (ψ = 0.40) and a single sphere (ψ = 1). This is due to the fact that the Reynolds numbers are considerably higher

for the technical product. Similar findings have been reported by various authors (see [10], among others).

Another important, though disappointing, difference from aluminum silicate is that we could not describe the entire fluid bed drying curves of the technical product by a constant NTU_g (or Sh_g). At the end of drying NTU_g had to be reduced by a factor of about 4 down to $NTU_{g2} = 0.3$, 0.6 and 0.9. In the region of medium solids moisture contents (at about $0.4 < X < 0.5$) linear interpolation between NTU_{g1} and NTU_{g2} has been practiced. Only in this way the characteristic shape of the fluid bed drying curves of Fig. 14 and the good agreement with the measurements could be attained.

We attribute this effect to the highly non-spherical shape of the particles in combination with the very large change of moisture content during drying. Note that initially about 1.2 kg water correspond to about 1 kg of the dry product. As a consequence, the particles experience a large change of their mass distribution and rotational momentum during drying. Because of particle shape rotational movement is very important in the fluid bed, so that a change of gas-side mass transfer kinetics may be anticipated during the drying phenomenon. On the other hand, a deviation between the particle-side kinetics measured with static or almost static particles (on the analytical balance or in the drying channel) and the drying kinetics of particles swept and turned around by the gas flow in the fluid bed is also probable.

The latter explanation would impact the validity of our scale-up and scale-down procedures as discussed in the introduction. However, it should be clearly kept in mind that our present technical product is rather exceptional. In the large majority of cases particles will be smaller, drier and more spherical. Consequently, most products will be rather like aluminum silicate and, thus, susceptible to the "double-scaling procedure".

CONCLUSION

Two aspects characterize the present work in comparison with previous literature:

- The concept of a normalized single particle drying curve has been integrated into a heterogeneous fluid bed model
- Drying curves have been measured for both single particles and fluid beds. Two different products have been used in the experimental investigations.

On this basis the following has been concluded:

- It is, in general, possible to predict fluid bed drying kinetics from normalized single particle data with the help of a fluid bed model.
- Difficulties arise with particles having a low sphericity and a large initial moisture content. Such particles may show a different drying behaviour when static than in the fluid bed.
- In the fluid bed model bubbling should be accounted for. Simpler versions (homogeneous, inactive bypass) are not sufficient.
- The ratio ν of air flow rate assigned to the bubbles as well as the number of units for mass transfer between the suspension and the bubbles NTU_1 which are necessary to predict our fluid bed data are well in the range indicated by general fluidization literature for these quantities.
- Sherwood numbers Sh_g for particle-to-fluid mass transfer in the fluid bed are, in the region of low Reynolds numbers, considerably smaller than the values valid for single particles.
- The above effect, which has been often reported in literature, is usually attributed to bypassing. This explanation does not appear to be satisfactory, since bubbling and bypassing have been explicitely accounted for in the present model.

ACKNOWLEDGMENTS

The author wishes to thank the Dow Chemical Company for permission to publish this paper; D. Hölder for carrying out the measurements in the course of his diploma work; and, Professor E.-U. Schlünder for providing experimental facilities for the single particle runs in his laboratory in Karlsruhe as well as for his general support and encouragement.

SYMBOLS

A	total particle surface area, m^2

A_b	total bubble surface area, m^2
d	particle diameter, m
h_0	static bed height (without fluidization), m
m_{fb}	drying rate of fluid bed, kg/(m^2h)
$m_{fb,s}$	fluid bed drying rate at saturation of outlet air, kg/(m^2h)
m_{fb}^*	reduced drying rate of fluid bed, eq.(5), -
m_{sp}	single particle drying rate, kg/(m^2h)
$m_{sp,I}$	single particle drying rate in the first drying period, kg/(m^2h)
M_g	mass flow rate of dry gas (air), kg/min
NTU_g	number of units for particle-to-fluid mass transfer, -
NTU_i	number of mass transfer units between suspension and bubble phase, -
$T_{g,in}$	inlet gas (air) temperature, K
u_0	superficial flow velocity, m/s
u_L	superficial velocity at incipient fluidization, m/s
γ	ratio of air flow through the bubble phase, -
ν_E	excess air flow ratio, eq.(6), -
X	solids moisture content, kg H_2O/kg dry solids
X_{cr}	critical moisture content, kg H_2O/kg dry solids
X_{eq}	equilibrium moisture content, kg H_2O/kg dry solids
β_g	mass transfer coefficient corresponding to NTU_g, m/s
β_i	mass transfer coefficient corresponding to NTU_i, m/s
δ	difusion coefficient, m^2/s
η	normalized solids moisture content, eq.(2), -
ν	normalized drying rate, eq.(1), -
ν_g	kinematic viscosity of gas, m^2/s
ρ_g	gas density, kg/m^3

REFERENCES

1. Reay, D. and Allen, R.W.K., 1982, Predicting the performance of a continuous well-mixed fluid bed dryer from batch tests, Proc. 3rd International Drying Symposium IDS'82, pp. 134-140.

2. Hoebink, J.H.B.J. and Rietema, K., 1980, Drying granular solids in fluidized bed, Chem. Eng. Sci., 35, Part I: pp. 2135-2140, Part II: pp 2257-2265.
3. Palancz, B., 1983, A mathematical model for continuous fluidized bed drying, Chem. Eng. Sci., 38 pp. 1045-1059.
4. Verkooijen, A.H.M., 1986, Fluidized bed drying of fine particles with internal diffusion limitation, Proc. 5th Engng Foundation Conf., Fluidization, pp. 643-650
5. Liedy, W. and Hilligardt, K., 1991, A contribution to the scale-up of fluidized bed driers and conversion from batchwise to continuous operation, Chem. Eng. Process., 30 pp. 51-58.
6. van Meel, D.A., 1958, Adiabatic convection batch drying with recirculation of air, Chem. Eng. Sci., 9 pp. 36-44.
7. Schlünder, E.-U., 1976, Fortschritte und Entwicklungstendenzen bei der Auslegung von Trocknern fur vorgeformte Trocknungsgüter, Chem.-Ing.-Tech, 48 pp. 190-198.
8. Zabeschek, G., 1977, Experimentelle Bestimmung und analytische Beschreibung der Trocknungsgeschwindigkeit rieselfähiger, kapillarporöser Güter in der Wirbelschicht, PhD-Thesis, Univ. of Karlsruhe.
9. Tsotsas, E., 1992, Measurement and modelling of intraparticle drying kinetics: A review, Proc. Eighth International Drying Symposium IDS'92, pp. 17-41.
10. Schwarzbach, J., 1989, Selektive Trocknung in der Wirbelschicht, PhD-Thesis, Univ. of Karlsruhe.
11. May, W.G., 1959, Fluidized-bed reactor studies, Chem. Eng. Progr., 55 pp. 40-56
12. Werther, J., 1984, Mathematische Modellierung von Wirbelschichten, Chem.-Ing.-Tech., 56 pp. 125-143.
13. Hölder, D., 1992, Diskontinuierliche Wirbelschichttrocknung: Aufbau und Erprobung einer Laborapparatur, Studie der Modellauswertung, Diploma thesis, Institut für Thermische Verfahrenstechnik, University of Karlsruhe
14. Davidson, J.F., Clift, R. and Harison, D. (eds), 1985, Fluidization, Academic Press, 2nd ed., London.
15. Geldart, D (ed.), 1986, Gas fluidization technology, John Wiley and Sons, New York.
16. Gnielinski, V., 1991, Wärmeübertragung Partikel-Fluid in durchströmten Haufwerken, VDI-Wärmeatlas, sect. Gh, VDI-Verlag, 6th ed., Düsseldorf.
17. Subramanian, D., Martin, H. and Schlünder, E.-U., 1977, Stoffübertragung zwischen Gas und Feststoff in Wirbelschichten, VT-Verfahrenstechnik, 11 pp. 748-750.

18. Tsotsas, E., 1992, On mass transfer, dispersion and macroscopical flow maldistribution in packed tubes, Chem. Eng. Process., 31 pp. 181-190